APL Materials

Examination of possible high-pressure candidates of $SnTiO_3$: The search for novel ferroelectric materials

Cite as: APL Mater. **9**, 021103 (2021); https://doi.org/10.1063/5.0029968
Submitted: 17 September 2020 . Accepted: 28 December 2020 . Published Online: 02 February 2021

Florian Pielnhofer, Leo Diehl, Alberto Jiménez-Solano, Annette Bussmann-Holder, J. Christian Schön, and Bettina V. Lotsch

Examination of possible high-pressure candidates of $SnTiO_3$: The search for novel ferroelectric materials

Cite as: APL Mater. 9, 021103 (2021); doi: 10.1063/5.0029968
Submitted: 17 September 2020 • Accepted: 28 December 2020 •
Published Online: 2 February 2021

Florian Pielnhofer,[1,2,a),b)] Leo Diehl,[1,3] Alberto Jiménez-Solano,[1] Annette Bussmann-Holder,[1] J. Christian Schön,[1] and Bettina V. Lotsch[1,3,a)]

AFFILIATIONS

[1] Max Planck Institute for Solid State Research, Heisenbergstr. 1, 70569 Stuttgart, Germany
[2] Institute of Inorganic Chemistry, University of Regensburg, 93040 Regensburg, Germany
[3] Department of Chemistry, Ludwig–Maximilians–Universität München, Butenandtstr. 5–13, 81377 München, Germany

[a)] **Authors to whom correspondence should be addressed:** florian.pielnhofer@ur.de and b.lotsch@fkf.mpg.de
[b)] **Present address:** Institute of Inorganic Chemistry, University of Regensburg, 93040 Regensburg, Germany.

ABSTRACT

Following the recent successful synthesis and characterization of bulk $SnTiO_3$, its energy landscape was studied by means of density functional theory, applying different exchange–correlation and hybrid functionals. Experimentally accessible structure candidates with composition ABX_3 were identified by a database search and global exploration approach. Besides the common octahedral coordination of Ti, also fourfold and fivefold coordination spheres emerged to be reasonable structural motifs. Among the predicted high-pressure modifications, the tetragonal perovskite structure turned out to be stable at pressures between 11 GPa and 15 GPa. The possibility of a paraelectric-to-ferroelectric phase transition of the tetragonal perovskite structure was investigated by modeling the phonon spectra and soft mode behavior. Despite substantial long wavelength transverse optical mode softening, the predicted high c/a-ratio in tetragonal perovskite $SnTiO_3$ inhibits the formation of a spontaneous reversible polarization.

I. INTRODUCTION

Recently, we reported about the first successful synthesis and the structural characterization of $SnTiO_3$ as a bulk material.[1] The structure can be understood as a heavily stacking-faulted variant of the expanded ilmenite-type structure, which was established by high resolution transmission electron microscopy (HRTEM) and X-ray powder diffraction (XRPD) investigations. The [α-$TlSbO_3$]-type accounts for this expansion, yet also does not fully describe the crystal structure of $SnTiO_3$ because of a different stacking sequence. Common to both structure types is the main structural motif of honeycomb layers of edge-sharing BO_6 octahedra that are decorated with A^{2+} cations. In order to understand the similarity between α-$TlSbO_3$ (space group $P\bar{3}1c$) and ilmenite (space group $R\bar{3}$), it is helpful to employ the hexagonal setting of the latter space group. Both structures are of (pseudo-)layered character, $P\bar{3}1c$ (α-$TlSbO_3$) being a double and $R\bar{3}$ (ilmenite) a triple layer cell, respectively. The lone pair of both Tl and Sn in α-$TlSbO_3$ and $SnTiO_3$, respectively, leads to an expansion into the stacking direction, which can be rationalized by the stereo-chemical activity of the lone pair electrons and differentiates them from the actual ilmenite-type structure. Therefore, $SnTiO_3$ and $FeTiO_3$ are not strictly isotypic but can be classified as isopuntal. We also use the [$FeTiO_3$] notation where applicable but add an "e" to explicitly emphasize that we mean the expanded ilmenite structure type. The weak out-of-plane interaction in $SnTiO_3$ induces stacking faults. To account for these faults, $SnTiO_3$ was described using five different polytype models that are also energetically quasi-identical[1] on the level of density functional theory (DFT).

Theoretical predictions on the most stable modification of $SnTiO_3$ had been discussed by Parker *et al.*[2] and Hautier *et al.*[3,4] before there was any experimental evidence. According to Parker,[2] the tetragonal perovskite structure with space group $P4mm$ is the ground state for $SnTiO_3$, whereas Hautier[3,4] predicted a distorted

ilmenite-type structure to be the thermodynamically stable form. It is, however, the perovskite-type structure of $SnTiO_3$ that is intensively discussed as a promising lead-free ferroelectric material among the solid state and materials science community, while neither the centrosymmetric e-[$FeTiO_3$] nor the [$FeTiO_3$]-type modification of $SnTiO_3$ is expected to show polar distortions.[5–14]

Experimental work by Fix *et al.*[15] has shown that also thin films of $SnTiO_3$ show a characteristic hexagonal diffraction pattern typical of the ilmenite-type structure. The lattice parameters of the thin film material show a distortion ($a \neq b$) due to substrate induced strain. The *c*-axis was determined to be 14.56 Å, which is 2/3 of our findings.[1] Despite the structural distortion, no ferroelectricity was observed. Based on weak reflections in XRPD reciprocal space maps, the authors further speculated about minor amounts of tetragonal perovskite $SnTiO_3$ present in the films.

Agarwal *et al.* and Chang *et al.*[5,16] even reported relaxor ferroelectricity in $SnTiO_3$ films grown on Si substrates by atomic layer deposition. They inferred to observe the presence of several crystallite orientations of perovskite-like structures with different *c*/*a* and *a*/*b* ratios. However, unambiguous conclusions concerning the crystal structure could not be drawn. Indeed, in a recent report, Gardner *et al.* revised their claims to have prepared perovskite-like $SnTiO_3$ due to a misinterpretation of experimental data.[17]

Recently, employing a low temperature flux-assisted method, O'Donnell *et al.* synthesized a solid solution series of perovskite type $Ba_{1-x}Sn_xTi_{1-y}Zr_yO_3$.[18] The highest amount of Sn(II) on the *A* site is found in $Ba_{0.4}Sn_{0.6}Ti_{0.5}Zr_{0.5}TiO_3$. Studies on the ferroelectric properties of these materials have not been reported yet.

The most prominent ferroelectrics[19] among the large family of perovskite materials[20] are Pb(Ti,Zr)O_3 and variants of $BaTiO_3$. Besides perovskites, the [$LiNbO_3$]-type structures exhibit high piezoelectric coefficients. Due to the center of inversion, compounds that crystallize in an ilmenite-type structure have to be excluded as candidate ferroelectrics. However, ABX_3 ilmenite-type titanates can be transformed into perovskite-type structures by applying high pressure, as has been demonstrated for (Mg,Fe)TiO_3,[21] $ZnTiO_3$,[22,23] and $CdTiO_3$,[24] the latter showing a ferroelectric phase transition at around 2 GPa and 600 °C. The phase transition to perovskite-type structures was observed in germanates, stannates ($CdSnO_3$), silicates, and even vanadates ($MnVO_3$).[25–28] In many cases, these phase transitions cannot be stabilized at room temperature, where the [$LiNbO_3$]-type phase is obtained instead,[29] which indeed has been proven to be ferroelectric.[30] To rationalize the observed effects under pressure, the Goldschmidt tolerance factor has been frequently used. This method is, however, inconclusive since it requires the knowledge of exact ionic radii, which, as already stated by Shannon,[31] are unreliable in the case of Sn^{2+} with reported values from 0.93 Å to 1.18 Å. If we nevertheless calculate a tolerance factor for $SnTiO_3$, it should lie in the range of 0.83–0.95, which typically corresponds to a ground state structure of rhombohedrally or orthorhombically distorted perovskites.

Lone pairs may induce, besides ferroelectricity, novel electronic properties under high pressure. For example, disproportionation in $PbCrO_3$ leads to an insulator-to-metal transition.[32] Generally, materials containing lone pairs have been shown to exhibit interesting anisotropic phase transitions.[33,34]

In light of the new experimental results presented recently by our group,[1] in this work, we reexamined the energy landscape of the $SnTiO_3$ system. More than 40 ABX_3 structure types were modeled at the *ab initio* level to identify experimentally accessible and possible ferroelectric modifications. Suitable structure candidates were chosen by a database search and global exploration approach. We predict two high-pressure modifications by equation of state (EoS) calculations. Phonon spectra for the predicted structures are calculated in order to check for the dynamical stability. Electronic and mechanical properties as well as viable ferroelectric phase transitions of the most promising candidates were investigated in detail.

II. METHODOLOGY

Structure optimization and total energy comparison for five different polytypes derived from the ilmenite-type structure have already been performed in our previous work.[1] The different stacking variants used for the structure determination from powder diffraction all exhibit very similar volumes per formula unit and differ in energy by at most 0.14 kJ mol^{-1} depending on the functional used for the modeling. These results are also employed in this work.

By evaluating all ABX_3 structures from the inorganic crystal structure database (ICSD) followed by local minimizations to identify kinetically stable candidate structures, a first overview of the energy landscape can be obtained.

To go beyond these known structure types, a global search routine—simulated annealing[35]—using a complex empirical potential as energy function as implemented in the G42+ code[36] was employed. In order to obtain reliable results for Sn^{2+}, it was required to use a dumbbell-like or puckered potential, which had already been successfully employed in the prediction of Sn(II) compounds.[37] The results from the database search and the global exploration approach were subsequently locally optimized at an *ab initio* level using the CRYSTAL code.[38–40] While the symmetry was restricted to the space group of the database structures, the models from the empirical potential landscape search were optimized in space group *P*1 and the real space group was determined afterward for the fully relaxed models with the symmetry and space group identification algorithms SFND[41] and RGS[42] implemented in the KPLOT software,[43] which is embedded in Endeavour.[44] In total, 44 structure types were modeled at DFT and hybrid level for $SnTiO_3$. A full list of the structure models investigated is given in the supplementary material (Tables S1–S3).

Energy vs volume curves were computed for all models, and the obtained data points were fitted to a Birch–Murnaghan EoS. The local optimizations on an *ab initio* level were performed within the local density approximation (LDA[45]), the generalized gradient approximation (GGA-PBE[46]), and the hybrid functional HSE06,[47] which contains 25% of the exact Fock exchange, as it is reasonable to compare different functionals in order to gain better insight in the quantitative validity of the results. We further compared the obtained results for the tetragonal perovskite structure (space group *P*4*mm*) with the GGA-based functionals (PBEsol and B1-WC), which had been shown to perform well with ferroelectric distortions[48] and especially in the context of super-tetragonality.[49]

III. RESULTS AND DISCUSSION

A. Structure models

As stated above, the experimentally observed structure can be represented by five different stacking variants as determined from

Rietveld refinement of powder diffraction data. The polytypes that were denoted with AB, ABC, ACB, ABCB, and ABCACB contain the prominent e-[$FeTiO_3$]-type structure (ABC) and the [α-$TlSbO_3$]-type structure (AB). Since the energy minima and volume per formula unit of the relaxed structures are almost identical (±0.1 kJ mol^{-1}; ΔV: ±0.3%) and all stacking variants can be derived from AB and ABC, the present study focuses on the e-[$FeTiO_3$] and [α-$TlSbO_3$] polytypes when comparing the experimental structures to the hypothetical structures. Among the (theoretical) structures investigated, the major differences can be found in the coordination spheres of Ti, which includes the perovskite-derivatives with (tilted/distorted) BX_6-octahedra and the silicate analogous structures with the tetrahedral *B*-site environment. To fully cover all possible *B*-site coordination environments, even a somewhat exotic fivefold coordination of *B* is modeled within the [$HgVO_3$]-type. A further differentiation can be made by comparing the different linkages of the polyhedra, which is corner-sharing in the perovskite-derivatives, while it is edge-sharing in e-[$FeTiO_3$] and [α-$TlSbO_3$] and face-sharing in the [$BaNiO_3$]-type, for example. All applied structure models are listed in Tables S1–S3. While the database search approach remains primarily controlled by chemical intuition, the predictive power of global structure searches has proven to be quite high in the recent past.[50,51] Employing *ab initio* DFT as an energy function during the global search proved to be problematic for the $SnTiO_3$ system due to convergence problems, and therefore, empirical potentials were used, which showed better performance. While hundreds of structure candidates for $SnTiO_3$ were found with the global search routine, only three of them could actually be locally optimized, again due to the convergence issues of the DFT code. However, one of the converged structure candidates exhibits similar chains of edge sharing BX_5 square pyramids as found in $HgVO_3$, thus proving the method to be chemically viable.

B. Energy landscape

In agreement with the study by Hautier *et al.*,[3,4] we find that the experimentally determined structure, which is indeed more complex than just ordinary e-[$FeTiO_3$] and [α-$TlSbO_3$] due to multiple stacking faults, is lowest in energy and, therefore, was identified as the most stable configuration for all applied functionals (HSE06 results are shown in Fig. 1). Here, PBE and HSE06 follow qualitatively the same trends, and LDA significantly differs in the magnitude of total energies. Results obtained by HSE06 perfectly reproduced the experimental lattice parameters *a* and c^*. Therefore, in this work, we present the HSE06-based results and only note the difference to LDA where required. Among the structure models found for $SnTiO_3$, the [PX-$PbTiO_3$][52,53] structure type is energetically closest to the e-[$FeTiO_3$]- and the [α-$TlSbO_3$]-type. This structure consists of edge-sharing one-dimensional octahedral TiO_6 chains (see Fig. 2) and has been realized for $PbTiO_3$ by hydrothermally treating slurries of soluble lead and titanium precursors.[54] This polymorph is predicted to be less stable by only +24.1 kJ mol^{-1} and exhibits a lower cell volume (67.46 $Å^3$) than the experimental one, thereby being energetically closest to experimental $SnTiO_3$.

Moreover, a structure with fivefold coordination of Ti, as present, for example, in the [$MgVO_3$]-type structure, is only +30.1 kJ mol^{-1} higher in energy and exhibits the largest cell volume within the probed structure types. The [$MgVO_3$]-type structure is built up from one-dimensional zigzag chains of edge-sharing TiO_5 quadratic pyramids.

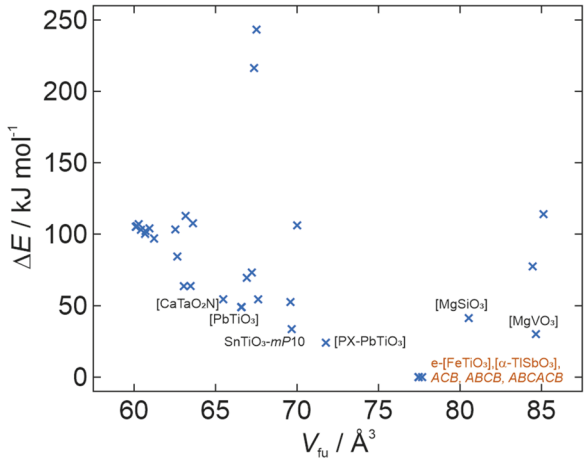

FIG. 1. Minima of energy vs volume plots of all modeled structure types for $SnTiO_3$ (HSE06 calculations).

A model with the same fivefold Ti coordination but another TiO_3 sublattice is found at +33.6 kJ mol^{-1} and 69.67 $Å^3$ ($SnTiO_3$-*mP*10). This model with space group $P2_1/m$ (no. 11) was predicted by the global search algorithm and features the same anionic double pyramidal chains, which are present in the [$HgVO_3$]-type, differing only in the stacking of the chains. This quadratic pyramidal coordination of Ti is realized also in the layered $K_2Ti_2O_5$ that served as a starting material when synthesizing $SnTiO_3$.[1] The actual [$HgVO_3$]-type is less favored for $SnTiO_3$ by another +20.9 kJ mol^{-1}. A tetrahedral coordination of Ti such as the one found in the [$MgSiO_3$]-type model leads to a large cell volume of 80.53 $Å^3$ and is energetically shifted by already +41.3 kJ mol^{-1} above the e-[$FeTiO_3$]- and [α-$TlSbO_3$]-type.

The desired candidate, the tetragonal perovskite-type structure ([$PbTiO_3$] with space group *P*4*mm*), is only the sixth most stable configuration for $SnTiO_3$ with an energy difference of +49.0 kJ mol^{-1}. It features, however, a lower cell volume (66.60 $Å^3$), suggesting a potential high-pressure transformation. Furthermore, the orthorhombic ($Pna2_1$), monoclinic (*Cm*, *Cc*), and triclinic versions of the perovskite-type structures converged to the same minimum of the energy hypersurface with exactly the same structure and symmetry (*P*4*mm*) within the error margin, indicating a large but not very deep basin in the energy landscape. The [$CaTaO_2N$]-type structure (SG $Pmc2_1$), which is also found at a lower cell volume (63.06 $Å^3$), is another representative of the large family of ABX_3 perovskites with only corner-sharing octahedra and is energetically unfavorable by +54.5 kJ mol^{-1}. The most stable structure types discussed are summarized in Table I (a full summary for all functionals is given in supplementary material, Tables S1–S3).

In materials with tolerance factors above $t = 0.8$ and below $t = 1$, often the [$GdFeO_3$]-type structure (SG *Pnma*) is found to be the ground state structure. For $SnTiO_3$, however, we find *Pnma* to be energetically destabilized by 97 kJ mol^{-1}, which is not uncommon for oxides containing lone pairs.[55,56]

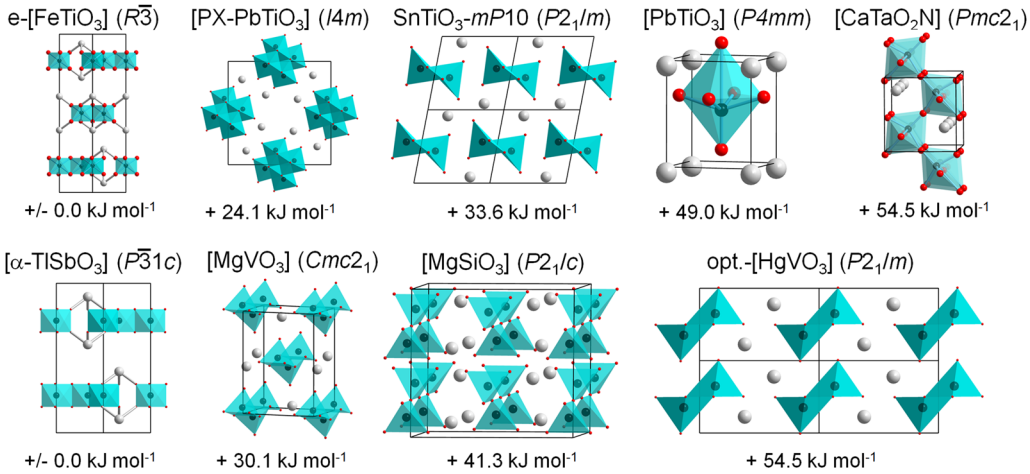

FIG. 2. Most stable predicted structure types and respective total electronic energies from HSE06 calculations (Sn: gray, Ti: black, and O: red). Note that the actual $[HgVO_3]$-type structure crystallizes in space group $P\bar{1}$, and the optimized $SnTiO_3$-model results in $P2_1/m$.

Face-sharing of TiO_6 octahedra in $SnTiO_3$ as modeled with the $[BaNiO_3]$-type is the least stable configuration of the probed structures (ΔE = +243.3 kJ mol^{-1}). The fact that most of the modeled hypothetic structures indeed exhibit lower cell volumes than the ground state $SnTiO_3$ suggests the possibility of pressure induced phase transitions. Therefore, all the E–V curves were fitted to equations of state and translated to ΔH vs p diagrams. Figure 3(b) shows the full range of stable high-pressure configurations up to 20 GPa. Indeed, the e-$[FeTiO_3]$- and $[\alpha$-$TlSbO_3]$-type $SnTiO_3$ show a phase transition to the tetragonal $[PbTiO_3]$-perovskite type at 11 GPa, and a further transition from this tetragonal perovskite to the $[CaTaO_2N]$-type is predicted at 15 GPa. Both pressures can routinely be realized in diamond anvil cells and even multi-anvil setups, thus making the experimental realization of these structures a realistic scenario. Note that no further high-pressure phases are predicted when increasing the pressure up to an extreme of 200 GPa.

In the following paragraph, we discuss the results of our proposed high-pressure phase transitions with regard to earlier theoretical work. Matar *et al.* predicted an a lattice parameter of 3.80 Å for the $[PbTiO_3]$ phase and a c/a ratio of 1.09 based on LDA calculations.[14] Parker *et al.* arrived at slightly larger c/a ratios of 1.13 (LDA) and 1.15 (WC-GGA).[2] The choice of the functional for reproducing experimental c/a values for tetragonal perovskites was intensively discussed for $PbTiO_3$ in Refs. 48 and 57. While LDA underestimates the c/a ratio, PBE and PBE0 overestimate it. The GGA of Wu and Cohen (WC-GGA), which had been applied to $SnTiO_3$ by Parker *et al.*,[2] as well as the improved PBE for solids (PBEsol), is in better agreement with the experimental values. Bilc *et al.* proposed the use of the alternative B1-WC functional that mixes the exact exchange with the WC-GGA.[48] This hybrid functional results in an accurate description of both the structural and electronic properties of $PbTiO_3$. In addition to LDA, PBE, and HSE06, we further applied the PBEsol, HSEsol, and B1-WC functionals to $PbTiO_3$ and $SnTiO_3$ in SG $P4mm$ to examine the validity of our results (see Tables S11 and S12). The hybrid GGAs PBEsol, HSEsol, and B1-WC predict similar lattice parameters for $PbTiO_3$ and slightly underestimate the tetragonality (see Table S11). The discrepancy for the c/a-ratio in $PbTiO_3$ between B1-WC (1.05) and HSE06 (1.14) is much larger than for $SnTiO_3$ (B1-WC: 1.17; HSE06: 1.21). Since both B1-WC

TABLE I. Energy difference to the most stable structure type and structural information (type, space group, volume per formula unit, and lattice parameters) for the most stable predicted structures for $SnTiO_3$ (HSE06 calculations).

Type	SG (no.)	ΔE (kJ mol^{-1})	$V Z^{-1}$ (Å^3)	a (Å)	b (Å)	c (Å)	β (deg)
e-$[FeTiO_3]$	$R\bar{3}$ (148)	0.0	77.46	5.07		20.86	
$[\alpha$-$TlSbO_3]$	$P\bar{3}1c$ (163)	0.0	77.68	5.07		13.94	
$[PX$-$PbTiO_3]$	$I4/m$ (87)	24.1	71.77	12.36		3.76	
$[MgVO_3]$	$Cmc2_1$ (36)	30.1	84.66	6.82	9.27	5.36	
$SnTiO_3$-$mP10$	$P2_1/m$ (11)	33.6	69.67				
$[MgSiO_3]$	$P2_1/c$ (14)	41.3	80.53	11.25	10.20	5.86	106.63
$[PbTiO_3]$	$P4mm$ (99)	49.0	66.60	3.80		4.60	
$[CaTaO_2N]$	$Pmc2_1$ (26)	54.5	65.47	7.45	5.85	6.02	
opt.-$[HgVO_3]$	$P2_1/m$ (11)	54.5	67.61	7.74	3.73	4.68	89.99

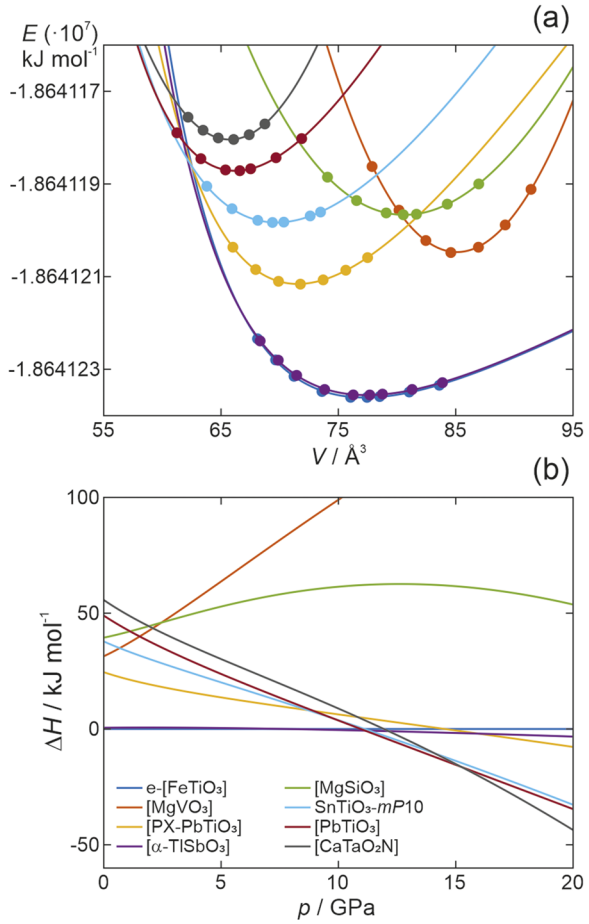

FIG. 3. (a) Energy vs volume curves and (b) ΔH vs p plots (HSE06 calculations).

and PBEsol furnish a very high c/a-ratio, we can conclude that a reasonable value for a potential $[PbTiO_3]$-type $SnTiO_3$ corresponds to an unusually large distortion. The underestimation of the c/a ratio for $PbTiO_3$ by B1-WC and the small difference of the latter to the HSE06 results for $SnTiO_3$ make HSE06 a reasonable functional for the structural description of $[PbTiO_3]$-type $SnTiO_3$. However, the functional for modeling a large number of unknown structure candidates for the same chemical composition has to be chosen with care. The starting point of our study—the structure of the only experimentally known bulk representative of $SnTiO_3$ (e-$[FeTiO_3]$-type or $[\alpha$-$TlSbO_3]$-type)—is perfectly reproduced with HSE06, which makes this hybrid our functional of choice for the whole energy landscape. Other perovskite-type compounds with extremely large c/a ratios have been reported as so-called supertetragonal phases.[49] In particular, $BiCoO_3$ and $PbVO_3$ reach values of over 1.2 for the c/a ratio. The consequence of the strong distortions in $[PbTiO_3]$-type $SnTiO_3$ will be discussed in Sec. III C 2. The shortest Ti–O distance in $[PbTiO_3]$-type $SnTiO_3$ obtained with HSE06 is 1.71 Å (B1-WC: 1.72 Å) and the longest is 2.90 Å (B1-WC: 2.72 Å). In contrast, $PbTiO_3$ (SG $P4mm$) has, for example, Ti–O distances of 1.79 Å and 2.36 Å. The relaxed structure (HSE06) of the second predicted high-pressure phase $[CaTaO_2N]$ (SG $Pmc2_1$) exhibits shortest and longest Ti–O distances at 1.77 Å and 2.82 Å, respectively, but still is more strongly distorted than tetragonal $PbTiO_3$.

To check if these strong distortions remain within the dynamic stability limits, both high-pressure phases were probed by calculating the phonon frequencies. Due to the very high computational costs with the hybrid functionals, the phonon spectra shown here (Fig. 4) were calculated at the PBE level. No physically relevant imaginary frequencies were obtained for both the $[PbTiO_3]$- and $[CaTaO_2N]$-type structures. Thus, realization of both phases by application of high hydrostatic pressure indeed seems feasible.

C. Properties

1. Electronic band structures and bulk modulus

Band structure calculations with the hybrid functionals HSE06 (Fig. 5) and B1-WC characterize both predicted high-pressure polymorphs as indirect gap semiconductors with slightly smaller bandgaps compared to tetragonal $PbTiO_3$ (PBE: 2.08 eV, expt. ~3 eV taken from Refs. 58 and 59). The calculated values for both theoretically predicted polymorphs of $SnTiO_3$, 1.87 eV for the $[PbTiO_3]$-type (B1-WC: 1.70 eV) and 1.95 eV for the $[CaTaO_2N]$-type (B1-WC: 1.94 eV), are very similar as expected due to a comparable bonding situation. The band structure for the $[PbTiO_3]$-type $SnTiO_3$ from Agarwal *et al.*[5] resembles the one presented in this work. Although they used the same hybrid functional HSE06, a slightly larger value of 2.175 eV for the indirect bandgap is predicted. Furthermore, the fitted EoS allow for the determination of bulk moduli B_0. The e-$[FeTiO_3]$-type structure has a very small B_0 of 24.0 GPa, which is typical for materials with weak interlayer bonding. In contrast, the bulk modulus of the first predicted HP-phase ($[PbTiO_3]$-type) is 59.4 GPa, and the second HP-phase ($[CaTaO_2N]$-type) has a B_0 of 82.9 GPa. This is reasonable since HP-polymorphs are generally less compressible than the standard pressure modifications.

2. Possible ferroelectricity

Within the family of perovskite titanates $ATiO_3$, various members are indeed ferroelectric ($BaTiO_3$ and $PbTiO_3$) or close to a ferroelectric instability ($SrTiO_3$ and $CaTiO_3$). In addition, mixed crystals of the type $A(B,B')O_3$ and $(A,A')BO_3$ may exhibit a ferroelectric ground state and in many cases show better performances than the undoped end members. It is quite generally agreed that a true ferroelectric instability stems from the oxygen-B-site cation

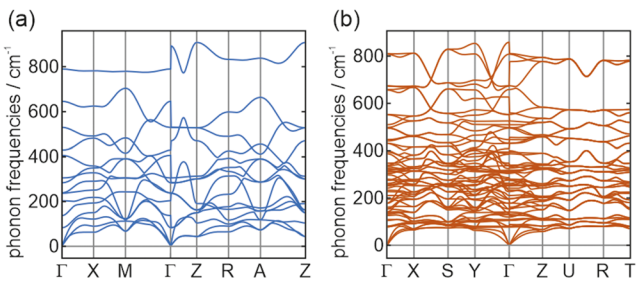

FIG. 4. Phonon dispersion relations of the (a) $[PbTiO_3]$-type ($P4mm$) and (b) $[CaTaO_2N]$-type ($Pmc2_1$) $SnTiO_3$ (PBE calculations).

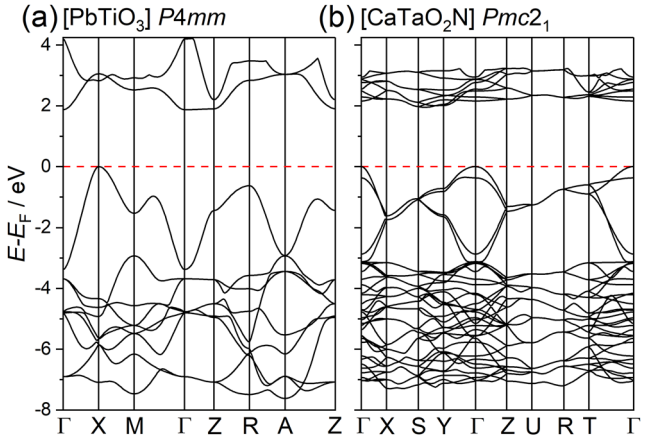

FIG. 5. Electronic band structures of (a) [$PbTiO_3$]-type and (b) [$CaTaO_2N$]-type $SnTiO_3$ (HSE06 calculations).

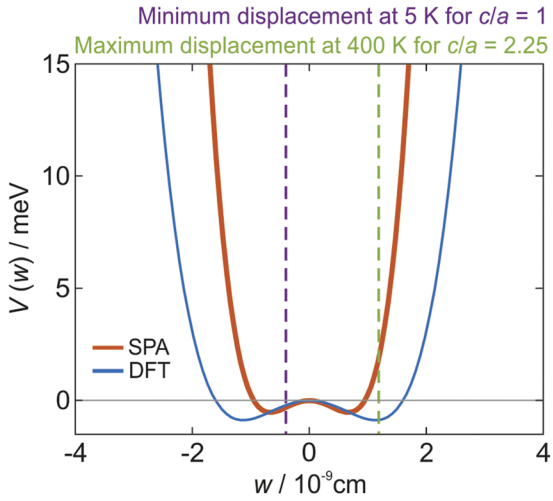

FIG. 6. Comparison of the double-well potentials of [$PbTiO_3$]-type $SnTiO_3$ as obtained within the self-consistent phonon approximation (SPA) and from DFT calculations. The double-well potential is plotted as a function of the polarizability displacement coordinate w. The red (blue) color refers to the $SnTiO_3$-related potential as obtained from the SPA (DFT). For details, see Ref. 63.

dynamical covalency where the A-site ion plays a significant role if it is involved through a lone pair.[60] We prefer the oxygen-B-site atom approach since in the revised lone pair model as elaborated in 2011 by Walsh *et al.*,[61] it was shown that lone pairs cannot be regarded as of pure cationic character but strongly incorporate/hybridize with the anionic oxide lattice. This is very analogous to $PbTiO_3$ where a substantial contribution to the polarization has been shown to stem from the oxygen-lead hybridized states.[62] A characteristic signature of a ferroelectric phase transition is the observation of the softening of a long wavelength transverse optical (TO) mode, which freezes out at the transition and determines the low temperature structural transformation. This is realized in both $BaTiO_3$ and $PbTiO_3$ but is incomplete in $SrTiO_3$ and $CaTiO_3$ due to quantum fluctuations in the former and negative transition temperatures in the latter. The modeling of mode softening in all compounds has been performed within the polarizability model,[20] which is based on a self-consistently derived double-well potential in the electron–ion interaction. In order to explore possible ferroelectricity in [$PbTiO_3$]-type $SnTiO_3$, we use exactly the same model; however, due to the lack of experimental data, this potential is taken to be the same as in $SrTiO_3$ (Fig. 6).

This choice is rather ambiguous but justifiable by the calculated a axis lattice parameter of [$PbTiO_3$]-type $SnTiO_3$, which is closest to the one of $SrTiO_3$. The A ion sublattice mass is replaced by Sn, whereas all other parameters are taken to be identical. Upon consideration of the hypothetical cubic structure type, a mode softening takes place in [$PbTiO_3$]-type $SnTiO_3$, which closely resembles the one of $SrTiO_3$ with an extrapolated T_c of 15 K, slightly smaller than the one of $SrTiO_3$ (Fig. 7). Quantum fluctuations set in around 35 K and inhibit a true instability. However, since the cubic structure is definitely not realized for $SnTiO_3$, we included the theoretically predicted tetragonal distortion for $P4mm$. For this, the c/a ratio is artificially enlarged while keeping the cell volume constant. All other parameters are identical to those in the undistorted compound. By increasing the c/a ratio, the soft mode frequency is stabilized, i.e., it adopts higher frequency values (as seen from the steeper slopes in Fig. 7), thereby shifting the extrapolated transition temperatures into the negative temperature regime, strongly disfavoring any ferroelectric instability.

In addition, and as expected from the enlarged c/a ratio, the dynamical relative Ti–O displacement w increases with the increasing c/a ratio—however, not linearly, but increasingly nonlinearly (Fig. 8), especially at high temperatures.

As indicated in Fig. 6 (dashed lines), even for the largest c/a ratio and highest temperature, the displacements are too small to escape the well to which they are confined. This observation implies that a frozen-in multi-domain state appears in the tetragonal phase where a switching between the two states by an electric field under ambient conditions is highly unlikely. The appearance of a reversible

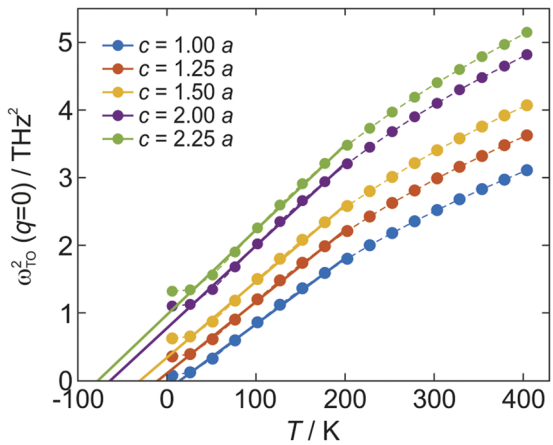

FIG. 7. The squared soft mode frequency $\omega^2_{TO}(q = 0)$ as a function of temperature for various c/a ratios as indicated. The thick lines are extrapolations of the linear temperature regions indicating possible transition temperatures.

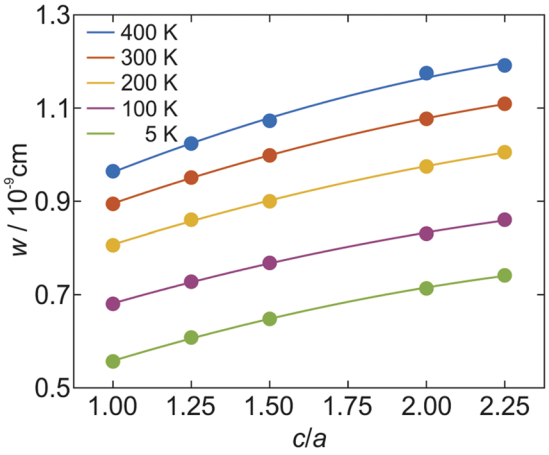

FIG. 8. Relative Ti–O displacement coordinate *w* as a function of the *c*/*a* ratio for 400 K, 300 K, 200 K, 100 K, and 5 K.

spontaneous polarization must thus be excluded. Here, it is important to emphasize that the observation of a polar space group is a necessary criterion for ferroelectricity, but not a sufficient one. A further requirement (see, e.g., the work of Lines and Glass[64]) is the reversibility of the spontaneous polarization, which in many polar structure types is not realized. From the results, it must be concluded that despite the possibility to have pronounced optical mode softening in $SnTiO_3$, even small tetragonal distortions rapidly suppress the appearance of a finite transition temperature. This is also true for the cubic phase where an instability is, however, suppressed by quantum fluctuations (nonzero ω^2_{TO} at 0 K). Possible applications of the predicted high-pressure phases of $SnTiO_3$ are nevertheless feasible since a large dielectric constant is expected, especially in the cryogenic temperature region. It is important to note that a number of unrealistic assumptions have been made in the above modeling: the double-well potential of $SrTiO_3$ has been used for the self-consistent derivation of the temperature dependence of the soft mode, a cubic structure has been taken as the starting point, and model parameters identical to those employed for $SrTiO_3$ have been used. Thus, these results have to be interpreted with care.

IV. CONCLUSIONS

We have explored the energy landscape of the compound $SnTiO_3$ and were able to confirm the earlier predictions that the expanded ilmenite-type structure is the most stable phase. We further predict two metastable high-pressure polymorphs: the [$PbTiO_3$]-type at pressures between 11 GPa and 15 GPa and the [$CaTaO_2N$]-type above p = 15 GPa. The existence of the [$PbTiO_3$]-type and its potential as a possible ferroelectric material have been intensively discussed in the literature. We predict a strong tetragonal distortion of the perovskite structure for $SnTiO_3$ as obtained with various GGA based functionals. This large distortion prevents a hypothetical tetragonal perovskite $SnTiO_3$ from polarity switching and entering a ferroelectric state. Hence, the phonon mode that describes the displacement of the Ti atom from the center of its octahedral environment cannot freeze out and thus excludes a ferroelectric instability.

SUPPLEMENTARY MATERIAL

See the supplementary material for further details on the DFT calculations and for optimized structures and energies.

ACKNOWLEDGMENTS

We thank the Computer Service Group at the Max Planck Institute for Solid State Research (Stuttgart, Germany) for providing computational facilities and Dr. Ulrich Wedig for his support in executing phonon calculations. Financial support by the DFG cluster of excellence e-conversion (EXC 2089/1-390776260) is gratefully acknowledged. A.J.-S. gratefully acknowledges a postdoctoral scholarship from the Max Planck Society.

DATA AVAILABILITY

The data that support the findings of this study are available from the corresponding author upon reasonable request.

REFERENCES

[1] L. Diehl, S. Bette, F. Pielnhofer, S. Betzler, I. Moudrakovski, G. A. Ozin, R. Dinnebier, and B. V. Lotsch, Chem. Mater. **30**, 8932 (2018).
[2] W. D. Parker, J. M. Rondinelli, and S. M. Nakhmanson, Phys. Rev. B **84**, 245126 (2011).
[3] G. Hautier, A. Jain, and S. P. Ong, J. Mater. Sci. **47**, 7317 (2012).
[4] G. Hautier, C. C. Fischer, A. Jain, T. Mueller, and G. Ceder, Chem. Mater. **22**, 3762 (2010).
[5] R. Agarwal *et al.*, Phys. Rev. B **97**, 054109 (2018).
[6] K. C. Pitike, W. D. Parker, L. Louis, and S. M. Nakhmanson, Phys. Rev. B **91**, 035112 (2015).
[7] T. Wang, K. C. Pitike, Y. Yuan, S. M. Nakhmanson, V. Gopalan, and B. Jalan, APL Mater. **4**, 126111 (2016).
[8] R. A. P. Ribeiro and S. R. de Lázaro, RSC Adv. **4**, 059839 (2014).
[9] R. A. P. Ribeiro and S. R. de Lazaro, J. Alloys Compd. **714**, 553 (2017).
[10] M. F. M. Taib, M. K. Yaakob, F. W. Badrudin, T. I. T. Kudin, O. H. Hassan, and M. Z. A. Yahya, Ferroelectrics **459**, 134 (2014).
[11] M. F. M. Taib, M. K. Yaakob, F. W. Badrudin, M. S. A. Rasiman, T. I. T. Kudin, O. H. Hassan, and M. Z. A. Yahya, Integr. Ferroelectr. **155**, 23 (2014).
[12] M. F. M. Taib, M. K. Yaakob, O. H. Hassan, and M. Z. A. Yahya, Integr. Ferroelectr. **142**, 119 (2013).
[13] H. Ye, R. Zhang, D. Wang, Y. Cui, J. Wei, C. Wang, Z. Xu, S. Qu, and X. Wei, Int. J. Mod. Phys. B **27**, 1350144 (2013).
[14] S. F. Matar, I. Baraille, and M. A. Subramanian, Chem. Phys. **355**, 43 (2009).
[15] T. Fix, S.-L. Sahonta, V. Garcia, J. L. MacManus-Driscoll, and M. G. Blamire, Cryst. Growth Des. **11**, 1422 (2011).
[16] S. Chang, S. K. Selvaraj, Y.-Y. Choi, S. Hong, S. M. Nakhmanson, and C. G. Takoudis, J. Vac. Sci. Technol., A **34**, 01A119 (2016).
[17] J. Gardner, A. Thakre, A. Kumar, and J. F. Scott, Rep. Prog. Phys. **82**, 092501 (2019).
[18] S. O'Donnell, C.-C. Chung, A. Carbone, R. Broughton, J. L. Jones, and P. A. Maggard, Chem. Mater. **32**, 3054 (2020).
[19] R. E. Cohen, Nature **358**, 136 (1992).
[20] A. Bussmann-Holder, J. Phys.: Condens. Matter **24**, 273202 (2012).
[21] A. Linton Jennifer, Y. Fei, and A. Navrotsky, Am. Mineral. **84**, 1595 (1999).
[22] M. Akaogi, K. Abe, H. Yusa, H. Kojitani, D. Mori, and Y. Inaguma, Phys. Chem. Miner. **42**, 421 (2015).
[23] Y. Inaguma, A. Aimi, Y. Shirako, D. Sakurai, D. Mori, H. Kojitani, M. Akaogi, and M. Nakayama, J. Am. Chem. Soc. **136**, 2748 (2014).

[24]J. Liebertz and C. J. M. Rooymans, Z. Phys. Chem. **44**, 242 (1965).
[25]L.-G. Liu, Earth Planet. Sci. Lett. **35**, 161 (1977).
[26]H. Yusa, M. Akaogi, N. Sata, H. Kojitani, R. Yamamoto, and Y. Ohishi, Phys. Chem. Miner. **33**, 217 (2006).
[27]H. Yusa, in *Nanoinformatics*, edited by I. Tanaka (Springer Singapore, Singapore, 2018), p. 259.
[28]K. Leinenweber, W. Utsumi, Y. Tsuchida, T. Yagi, and K. Kurita, Phys. Chem. Miner. **18**, 244 (1991).
[29]A. Navrotsky, Chem. Mater. **10**, 2787 (1998).
[30]T. Varga *et al.*, Phys. Rev. Lett. **103**, 047601 (2009).
[31]R. D. Shannon, Acta Crystallogr., Sect. A **32**, 751 (1976).
[32]J. Cheng *et al.*, Proc. Natl. Acad. Sci. U. S. A. **112**, 1670 (2015).
[33]J. Zhang *et al.*, J. Phys. Chem. C **115**, 020710 (2011).
[34]L. A. Olsen, T. Balić-Žunić, and E. Makovicky, Inorg. Chem. **47**, 6756 (2008).
[35]S. Kirkpatrick, C. D. Gelatt, and M. P. Vecchi, Science **220**, 671 (1983).
[36]J. C. Schön, Process. Appl. Ceram. **9**, 157 (2015).
[37]C. Mellot-Draznieks, S. Girard, G. Férey, J. C. Schön, Z. Cancarevic, and M. Jansen, Chemistry **8**, 4102 (2002).
[38]R. Dovesi, R. Orlando, B. Civalleri, C. Roetti, V. R. Saunders, and C. M. Zicovich-Wilson, Z. Kristallogr.–Cryst. Mater. **220**, 571 (2005).
[39]R. Dovesi *et al.*, Int. J. Quantum Chem. **114**, 1287 (2014).
[40]R. Dovesi *et al.*, *CRYSTAL14 User's Manual* (University of Torino, Torino, 2014).
[41]R. Hundt, J. C. Schön, A. Hannemann, and M. Jansen, J. Appl. Crystallogr. **32**, 413 (1999).
[42]A. Hannemann, R. Hundt, J. C. Schön, and M. Jansen, J. Appl. Crystallogr. **31**, 922 (1998).
[43]R. Hundt, *KPLOT - A Program for Plotting and Analyzing Crystal Structures* (Technicum Scientific Publishing, Stuttgart, Germany, 2016).
[44]H. Putz, J. C. Schön, and M. Jansen, J. Appl. Crystallogr. **32**, 864 (1999).
[45]S. H. Vosko, L. Wilk, and M. Nusair, Can. J. Phys. **58**, 1200 (1980).
[46]J. P. Perdew, K. Burke, and M. Ernzerhof, Phys. Rev. Lett. **77**, 3865 (1996).
[47]J. Heyd, G. E. Scuseria, and M. Ernzerhof, J. Chem. Phys. **118**, 8207 (2003).
[48]D. I. Bilc, R. Orlando, R. Shaltaf, G. M. Rignanese, J. Íñiguez, and P. Ghosez, Phys. Rev. B **77**, 165107 (2008).
[49]N. Cohen and O. Diéguez, Isr. J. Chem. **60**, 833 (2020).
[50]M. Addicoat *et al.*, Faraday Discuss. **211**, 325 (2018).
[51]M. Jansen and J. C. Schön, in *Comprehensive Inorganic Chemistry II*, 2nd ed., edited by J. Reedijk and K. Poeppelmeier (Elsevier, Amsterdam, 2013), p. 941.
[52]J. Wang *et al.*, Nat. Mater. **14**, 985 (2015).
[53]J. Wang *et al.*, Chem. Mater. **23**, 2529 (2011).
[54]H. Cheng, J. Ma, Z. Zhao, D. Qiang, Y. Li, and X. Yao, J. Am. Ceram. Soc. **75**, 1123 (1992).
[55]O. Diéguez, O. E. González-Vázquez, J. C. Wojdeł, and J. Íñiguez, Phys. Rev. B **83**, 094105 (2011).
[56]O. Diéguez and J. Íñiguez, Phys. Rev. B **91**, 184113 (2015).
[57]G. Sophia, P. Baranek, C. Sarrazin, M. Rérat, and R. Dovesi, Phase Transitions **86**, 1069 (2013).
[58]A. Stashans, C. Zambrano, A. Sanchez, and L. M. Procel, Int. J. Quantum Chem. **87**, 145 (2002).
[59]L. Wang, P. Yuan, F. Wang, E. Liang, Q. Sun, Z. Guo, and Y. Jia, Mater. Res. Bull. **49**, 509 (2014).
[60]A. Bussmann-Holder and H. Böttner, Nature **360**, 541 (1992).
[61]A. Walsh, D. J. Payne, R. G. Egdell, and G. W. Watson, Chem. Soc. Rev. **40**, 4455 (2011).
[62]Y. Shen, J. Cai, H.-C. Ding, X.-W. Shen, Y.-W. Fang, W.-Y. Tong, X.-G. Wan, Q. Zhao, and C.-G. Duan, Adv. Theory Simul. **2**, 1900029 (2019).
[63]J. L. Bettis, M.-H. Whangbo, J. Köhler, A. Bussmann-Holder, and A. R. Bishop, Phys. Rev. B **84**, 184114 (2011).
[64]M. E. Lines and A. M. Glass, *Principles and Applications of Ferroelectrics and Related Materials* (OUP Oxford, 2001).